Journal of The Electrochemical Society, 2021 **168** 113502
1945-7111/2021/168(11)/113502/7/$40.00 © 2021 The Electrochemical Society ("ECS"). Published on behalf of ECS by IOP Publishing Limited

Unraveling the Role of Water on the Electrochromic and Electrochemical Properties of Nickel Oxide Electrodes in Electrochromic Pseudocapacitors

Kun Wang,[1,3] Hongliang Zhang,[1,2,z] Weiping Xie,[1] Guoxin Chen,[1] Ran Jiang,[3] Kai Tao,[3] Lingyan Liang,[1] Junhua Gao,[1] and Hongtao Cao[1,2,z]

[1]*Laboratory of Advanced Nano Materials and Devices, Ningbo Institute of Materials Technology and Engineering, Chinese Academy of Sciences, Ningbo 315201, People's Republic of China*
[2]*Center of Materials Science and Optoelectronics Engineering, University of Chinese Academy of Sciences, Beijing 100049, People's Republic of China*
[3]*Institute of Inorganic Materials, School of Materials Science and Chemical Engineering, Ningbo University, Ningbo 315211, People's Republic of China*

Although nickel oxide (NiO) is currently the most promising for industrialization as a counter electrode, it has proven challenging to achieve long-term-stable electrochromic devices. One of the crucial components is the mechanism of action of water on the active interface of the NiO counter electrode in the Li^+-based electrolyte, which gives a basis of determinants for improving long-term cycling stability in devices. Herein, we investigate the role of water on the electrochemical and electrochromic properties of nickel oxide (NiO) electrodes. The finding of improved pseudocapacitive characteristics and reaction kinetics of NiO electrodes after introducing H_2O into the Li^+-based electrolyte can be originated from the increase of the number of ions and reduction of the electrolyte resistance and the interfacial charge-transfer resistance. On the one hand, the mechanisms for improved electrochemical and electrochromic properties such as a high coloration efficiency of 157.58 $cm^2\ C^{-1}$ under the potential window of ±1.4 V, an excellent rate capability and a superior long-term cycling stability of over 10,000 cycles in the ESCs based on WO_3 and NiO electrodes are elaborated. On the other hand, electrical water splitting can give rises to a degradation of optically cyclic stability of the NiO-based ESCs under the potential of $> +1.23$ V. These results provide a significant contribution to the reversibility and stability of the active interfaces for high performance electrochromic devices.
 [DOI: 10.1149/1945-7111/ac3527]

Manuscript submitted August 12, 2021; revised manuscript received October 20, 2021. Published November 11, 2021.

Supplementary material for this article is available online

At present, due to the excessive consumption of resources and destruction of the environment, energy saving and emission reduction have been receiving considerably increasing attention for the past two decades.[1,2] The innovation of energy storage materials and technologies greatly advances the investigation and exploitation of devices based on energy conversion, storage and conservation such as electrochromic supercapacitor, solar cell and lithium-ion battery.[3,4] Supercapacitors have been considered as the most promising candidates for energy storage mainly on account of their high capacitances, fast recharge capability, good cycling stability, long lifetime and environmental friendliness.[5–7] As a type of supercapacitors, pseudocapacitors store energy through fast and highly reversible surface or near-surface redox reactions.[8] Interestingly, both electrochromic supercapacitors and pseudocapacitors generally own sandwich-like device configurations and store energy in the same way.[9] Significantly, energy status of electrochromic supercapacitors could be visually monitored by the color change during the process of charge and discharge.[10–14] Thus, it would be greatly appealing to research the high-performance electrochromic pseudocapacitors (ESCs) with the functions of electrochromism and energy storage.

During the last decade, electrochromic pseudocapacitive materials have attracted tremendous focus on the abilities to change reversibly their colors or optical properties (absorbance/transmittance/reflectance) via a small external voltage or current change.[15,16] The typical materials include transition metal oxides (NiO,[17,18] WO_3,[19,20] PB[21,22] and V_2O_5[23]) and conductive polymers (polyaniline[24]). Among these materials, NiO is considered as a promising oxide for ESCs due to its high theoretical capacitance value and excellent chemical stability.[25] The pseudocapacitive characteristics of NiO counter electrodes depend mainly on their crystallinity, morphology and conductivity.[26] In order to improve its pseudocapacitive characteristics, several methods such as adjusting constructions, preparing composites and introducing dopants have been tried.[27] For instance, hydrothermally synthesized NiO electrodes enjoy excellent rate capability, large optical modulation and high coloration efficiency.[28] Kim et al. improve the electrochemical properties of the ESCs by doping copper (Cu) into the NiO film to reduce the charge transfer resistance and sheet resistance.[29] The conductivity of NiO thin films prepared by reactive sputtering is considered to be increased with the introduction of H_2O into reaction O_2 precursor gas.[30,31] In fact, crystal water of the NiO counter electrode or water-doped in the Li^+-based electrolyte becomes one of the crucial components for ESCs.[32] However, the effect of water on the electrochemical and electrochromic properties of NiO electrodes has yet to be unraveled.

Herein, we examine the potential role that water in the Li^+-based electrolyte can play in improving the electrochemical and electrochromic properties of the NiO electrodes for ESCs. Our observations confirm that the electron beam evaporated NiO thin films show an improved pseudocapacitive characteristics and reaction kinetics by incorporating H_2O into the Li^+-based electrolyte. Electrically driven water splitting under the potential of $> +1.23$ V can contribute chiefly to the irreversible degradation of the NiO electrodes in the complementary WO_3-NiO ESCs, as depicted in Fig. 1.

Experimental

Preparation of thin films and electrochromic device assembly.—The NiO thin films were deposited on the ITO-coated glass by electron beam evaporation technique (MUE-ECO made in ULVAC, Japan). Several pure NiO particles with the diameter of ~3 mm in a tungsten crucible were bombarded by an electron beam of 10 kV in the vacuum of 2×10^{-3} pa with a deposition rate of 0.1 nm s^{-1} and a thickness of 300 nm. Subsequently, these samples were annealed respectively at 300 °C for 1 h at a rate of 5 °C min^{-1} in air. Similarly, the 300 nm thick WO_3 thin films were deposited on the ITO-coated glass at a substrate temperature of 200 °C by electron beam evaporation technique. The complementary ESCs with

[z]E-mail: zhanghl@nimte.ac.cn; h_cao@nimte.ac.cn

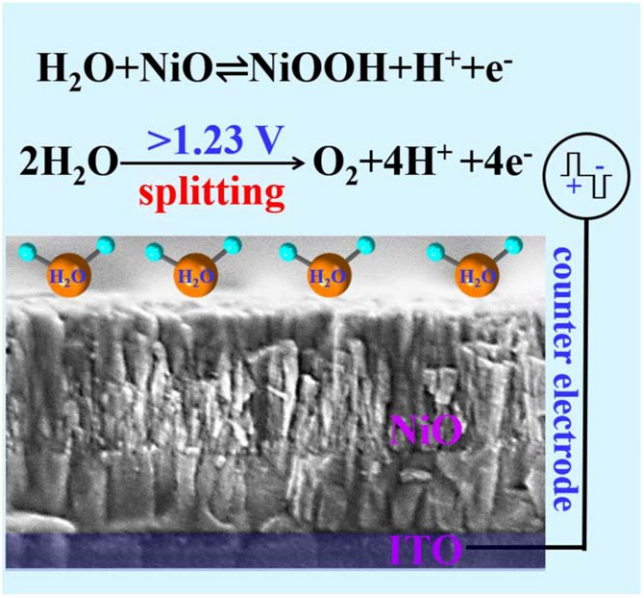

Figure 1. A schematic diagram of effects of electrical water splitting on the ESCs.

ITO/NiO/Li^+-based electrolyte/WO_3/ITO configuration were assembled by injecting 0.1 M Li^+ electrolytes without and with H_2O (volume ratio of electrolyte and water is fixed at 10:1 and 100:1) in between glass/ITO/NiO and WO_3/ITO/glass substrates in the vacuum filling process described elsewhere.[33]

Characterizations.—The phase structures of the as-deposited NiO thin films were checked by X-ray diffraction (XRD, Bruker D8 Advance using Cu-Kα (λ = 0.154178 nm) radiation and a θ–2θ configuration). The morphologies were analyzed by thermal field-emission scanning electron microscopy (TFESEM; Verios G4 UC, Thermo Scientific, USA). Electrochemical measurements of the films were carried out by an electrochemical workstation (CHI660D, Chen hua Shanghai) in a three-electrode cell where a platinum sheet as counter electrode, KCl saturated $Hg/HgCl_2$ as a reference electrode and 0.10 M $LiClO_4$-PC electrolytes without and with H_2O as the electrolyte, respectively. The electrochemical impedance spectra of the NiO thin films were recorded using an electrochemical workstation (Zennium, IM6) in the frequency range from 100 mHz to 100 kHz. Electrochromic properties of the ESCs were measured via UV–vis-IR spectroscopy (PerkinElmer Lambda 950) and an electrochemical workstation (CHI660D, Chen hua Shanghai). Galvanostatic charge-discharge (GCD) tests of the ESCs were performed using an electrochemical workstation (Zennium, IM6) at different current densities.

Results and Discussion

Electrochemical properties of the NiO thin films.—The cyclic voltammetry curves of the NiO thin films in 0.1 M Li^+-based electrolytes without and with H_2O at different scan rate range from 10 mV s^{-1} to 100 mV s^{-1} between 0.00 V and +1.20 V are shown in figure S1a, Figs. 2a and S1b, respectively. The peak value of the current density of the NiO thin films increases in accordance with the increase of the scan rate. It can be observed that the peak value of the NiO thin films in electrolytes with H_2O is larger than that without H_2O at the same scan rate, which indicates the faster redox reactions and the lower resistance at the active interface after introduction of H_2O.[34] These results can be attributed to the reaction between H_2O and NiO as the following equation:[35]

$$\text{NiO (bleached)} + H_2O \leftrightarrow \text{NiOOH(colored)} + H^+ + e^- \quad [1]$$

The switching speed of the ESCs is mainly dependent on the diffusion coefficient and the diffusion distance of ions.[36] The diffusion coefficient is calculated according to the Randles−Sevcik equation:

$$i_p = 2.69 \times 10^5 n^{3/2} A D^{1/2} C v^{1/2} \quad [2]$$

where i_p, n, A, D, C and v refer to the peak current, the number of electrons in the reactions, the contract area between the active interface and the electrolyte, the diffusion coefficient, the ion concentration and the scan rate, respectively.[37] Generally, the radii and the charge feature of ions are believed to be closely related to the diffusion coefficient.[38] The value of the respective calculated diffusion coefficient is about 1.02×10^{-16}, 2.14×10^{-14} and 6.46×10^{-14} cm^2 s^{-1} in the electrolyte without and with H_2O, as shown in Fig. 2b. The large value is related to the porous structure of NiO films (see S2 in the Supporting Information). Furthermore, the increase of the diffusion coefficient implies the introduction of water into the Li-based electrolyte leads to more ions including Li^+, H^+ and electron at the active interface of NiO/electrolyte. In Fig. 2c, the maximum charge density is determined to be 2.80 mC cm^{-2} (without H_2O), 4.67 mC cm^{-2} (volume ratio of electrolyte and water is 100:1) and 8.48 mC cm^{-2} (volume ratio is 10:1), suggesting the improvement of charge capacity with addition of H_2O into the electrolyte. In addition, the reversibility of the NiO thin films can be analyzed by the following equation:[39]

$$\text{Reversibility} = \frac{Q_{ex}}{Q_{in}} \times 100\%. \quad [3]$$

Where Q_{ex} and Q_{in} are the extracted and inserted charge. According to Fig. 2c, the reversibility is reduced from 96.97% (100:1) to 79.28% (10:1), indicating the excessive introduction of water into the Li-based electrolyte can cause the cyclic reversibility to deteriorate more seriously, and the moderate introduction of water (100:1) can improve the cyclic reversibility. To further identify the faradaic and capacitive-controlled processes, the "b" value is analyzed by the following equation:[40]

$$i = av^b \quad [4]$$

where a and b represent two variable parameters and v refers to the sweep rate, respectively. A "b" value of 1.0 is generally deemed to represent a capacitive controlled process. As shown in Fig. 2d, the "b" value of the NiO thin films is calculated respectively to be approximately 0.95, 0.96 and 1.19, suggesting that the dominance of the surface-controlled (capacitive) electrochemical reaction is increased with the addition of water into the Li-based electrolyte. To reveal the surface-capacitive effect, the capacitive (k_1v) and diffusion-controlled ratio($k_2v^{(1/2)}$) are obtained by the following equation:[41]

$$i(V) = k_1 v + k_2 v^{\frac{1}{2}} \quad [5]$$

where i and v represent a current at a certain potential of V and the scan rate, respectively. As illustrated in Figs. 2e and 2f, the surface-capacitive effect becomes gradually dominant with the increase of the scan rate. It can be found obviously that the capacitive contribution of the NiO thin films in the Li^+-based electrolyte with H_2O by volume ratio of 100:1 is more than that by volume ratio of 10:1 at the same scan rate, suggesting that the moderate addition of water (100:1) is beneficial to the improvement of the pseudocapacitive contribution. The more pseudocapacitive contribution is in favor of good cycling stability,[42] in line with the improvement of cyclic reversibility above.

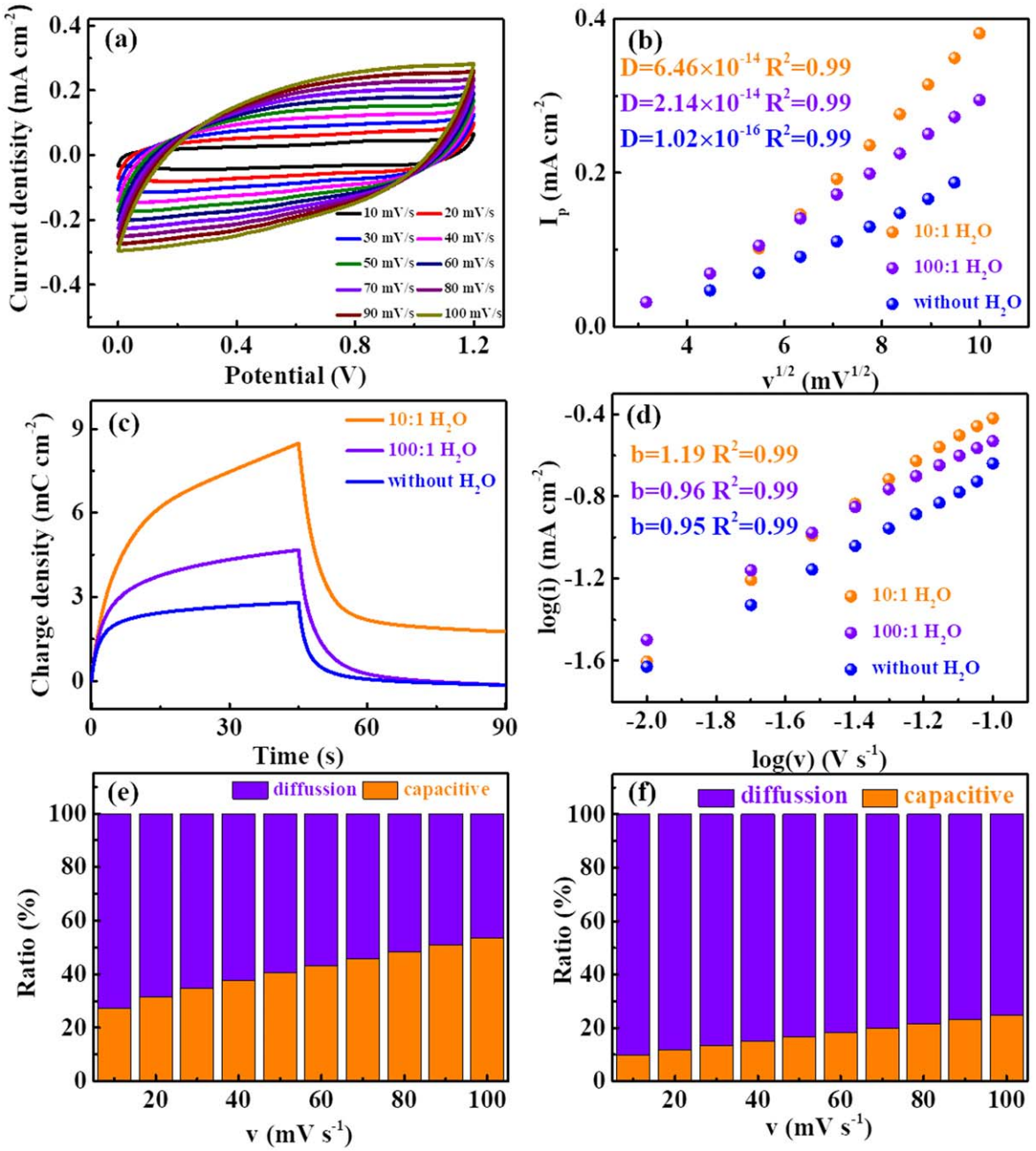

Figure 2. Cyclic voltammograms with a potential range of 0.0 to +1.2 V at scan rate from 10 to 100 mV s^{-1} for NiO films in the PC-$LiClO_4$ electrolyte (a) with H_2O (volume ratio 100:1). (b) Dependence of the peak current densities (Ip) versus the square root of scan rate ($v^{1/2}$), (c) charge density and (d) the power law relationship between peak current and scan rate for the NiO thin films in the three electrolytes.(f) The separation of contributions from capacitive and diffusion-controlled process as a function of processes at different scan rates for the NiO thin films in 0.10 M PC-$LiClO_4$ with H_2O (volume ratio 100:1 and 10:1).

Electrochemical impedance spectra.—Nyquist plots of the NiO thin films at the bleached and colored state in the Li^+-based electrolyte with and without H_2O in the frequency region ranging from 100 mHz to 100 kHz are displayed in Figs. 3a and 3b. The Randles equal circuit model is used to characterize the EIS data, as shown in the inset of Fig. 3a. The resistance (R_s) of the electrolyte and the interfacial charge-transfer resistance (R_{ct}) is determined by the intercept of the real axis in the high frequency region and the diameter of the semicircle in the high-frequency region, respectively.[43] The fitted values based on the analysis of electrochemical impedance spectra are given in Table I. During the oxidation/reduction reaction, anion insertion/extraction (OH^-) and cation extraction/extraction (Li^+&H^+), as reported previously.[18] The introduction of water into the Li-based electrolyte can lead to a decrease of R_s, indicating that the NiO thin films in the Li^+ electrolyte with H_2O possesses a higher ionic conductivity. The R_{ct} related to the charge-transfer during the redox reaction is observed to decrease gradually at +1.20 V with the addition of water, which can be ascribed to the promoted chemical reaction of Eq. 1. When a potential of 0.00 V is applied to the NiO counter electrode, the fitted value of R_{ct} decreases first and then increases with the increase of the content of H_2O in the electrolyte, suggesting that excessive introduction of water into the electrolyte can inhibit the reduction reaction of Eq. 1. Therefore, the NiO counter electrodes enjoy a higher reversibility in a moderate concentration of water-doped Li^+-based electrolyte (volume ratio of 100:1), consistent with the reversibility calculated above.

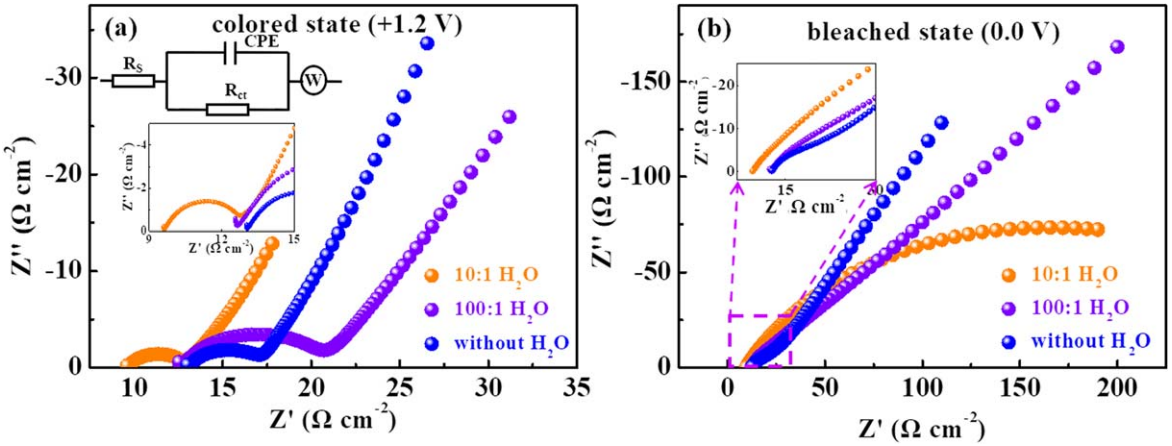

Figure 3. Nyquist plots measured for the NiO films in PC-$LiClO_4$ electrolyte without and with H_2O (volume ratio 100:1 and 10:1) at (a) 1.2 V and (b) 0.0 V.

Table I. A summary of Nyquist measurement for the NiO thin films in PC-$LiClO_4$ electrolyte without and with H_2O (volume ratio 100:1 and 10:1).

	Electrical Parameters					
Applied Potentials	R_s (Ω cm^{-2})			R_{ct} (Ω cm^{-2})		
(V)	100:1	10:1	without H_2O	100:1	10:1	without H_2O
0.00	14.44	16.80	22.58	5.29	107.59	284.88
+1.20	15.12	16.87	24.87	5.89	3.19	972.68

Electrochromic performance of the ESCs.—Electrochromic performance of the complementary WO_3-NiO ESCs based on the moderate concentration of water-doped Li^+-based electrolyte are further investigated as follows. Figures 4a–d displays in situ transmittance of the ESCs at 633 nm by applying alternately different potential window of ±1.0 V, ±1.1 V, ±1.2 V and ±1.3 V with a cycle period of 100 s, respectively. It can be observed obviously that the optical modulation gradually increases with increasing the potential window. After 100 cycles, the optical transmittance modulation of the ESCs under the potential window of ±1.3 V drops by 4.5%, higher than that of the ESCs under the potential window of ±1.0 V, ±1.1 V and ±1.2 V, where the degradation value of optical modulation performance is less than or equal to 1.3%. The possible reasons for the degradation of optical modulation performance are as follows. First, more ions (H^+ from ionization of water) caused by a higher potential window of ±1.3 V can inhibit the reversible chemical reaction of Eq. 1. Second, the effect of electric water splitting can give rises to the performance of the water-doped Li^+-based electrolyte to degrade due to the higher potential window of more than 1.23 V.[44] Third, the excessive insertion of H^+ into the active interface of the WO_3 thin films can result in the reversible degradation of the electrochromic and electrochemical performance in the complementary WO_3-NiO ESCs. According to in situ spectra analysis of the first 10 cycles of the ESCs with the various potential windows in Fig. 4e, the transmittance variety of the colored state of the ESCs is greater than that of the bleached state. The optical transmittance modulation (ΔT) increases from 22.0% of the potential window of ±1.0 V to 39.6% of the potential window of ±1.5 V. Moreover, the bleached response time of the complementary WO_3-NiO ESCs decreases from 7 s to 4 s with the applied voltage from $<$ 1.23 V to $>$ 1.23 V, and their colored response time possess almost the same value of 12 s. Figure 4 f displays the plots of in situ optical density variation as a function of charge density at λ_{633} nm of the complementary WO_3-NiO ESCs under the different potential windows. The fitted value of the coloration efficiency (η) for the ESCs is distributed between 89.60 cm^2 C^{-1} and 157.58 cm^2 C^{-1}, higher than that (65.11 cm^2 C^{-1}) of complementary WO_3-NiO ESCs without H_2O in our previous study.[45]

Capacitor Performance of the ESCs.—In order to assess the performance of the complementary WO_3-NiO ESCs, a series of CV curves and the charge/discharge curves under various potential windows is given in Fig. 5. The similar shape for the CV curves at all potential windows from ±1.0 V to ±1.5 V is shown in Fig. 5a, indicating the good stability of ESCs.[46] On the basis of the charge and discharge curves, the areal capacitances of the ESCs as a function at various current densities from 0.05 to 0.1 mA cm^{-2} under different potential windows are summarized in Figs. 5b and 5c. It can be observed that the areal capacitances gradually increase at the same current density with the enlarged voltage windows. The fastest areal capacitance drop (from 0.73 mF cm^{-2} at 0.05 mA cm^{-2} to 0.61 mF cm^{-2} at 0.1 mA cm^{-2}) can be seen under the potential window of ±1.1 V. The capacitance retention is still as high as 82.98%, which can be due to the low ion diffusion resistance at the active interface and the low electrolyte resistance, as reported previously.[47] In addition, the capacitance retention ratio after 10,000 cycles can be calculated to be about 104.24% for the ESCs under the potential window of ±1.1 V (in Fig. 5d), which can be ascribed to the activation at the active interface[48] and the better charge matching between two electrodes after the addition of H_2O.

Mechanism of action of H_2O.—The mechanisms of reversible reaction and electrochromic degradation at the active interface between the NiO electrode and the water-doped Li^+-based electrolyte are illustrated in Fig. 1. On the one hand, the introduction of water into the Li^+-based electrolyte leads to faster redox reactions and higher diffusion coefficient, which can be due to the lower resistance of the electrolyte and the interfacial charge-transfer resistance on the basis of the aforementioned EIS results. On the other hand, reversibility and pseudocapacitive contribution of the NiO films can be improved owing to the redox reaction between NiO and H_2O. Furthermore, H^+ generated by the reaction of Eq. 1 can move together with Li^+ in orientation under the electric potential and take part in the electrochromic reaction of the WO_3 films, which not only provides more ions to insert, but also enhances the electrochromic performance of the WO_3 electrode.[49] Based on these observations, we are convinced that our understanding of the

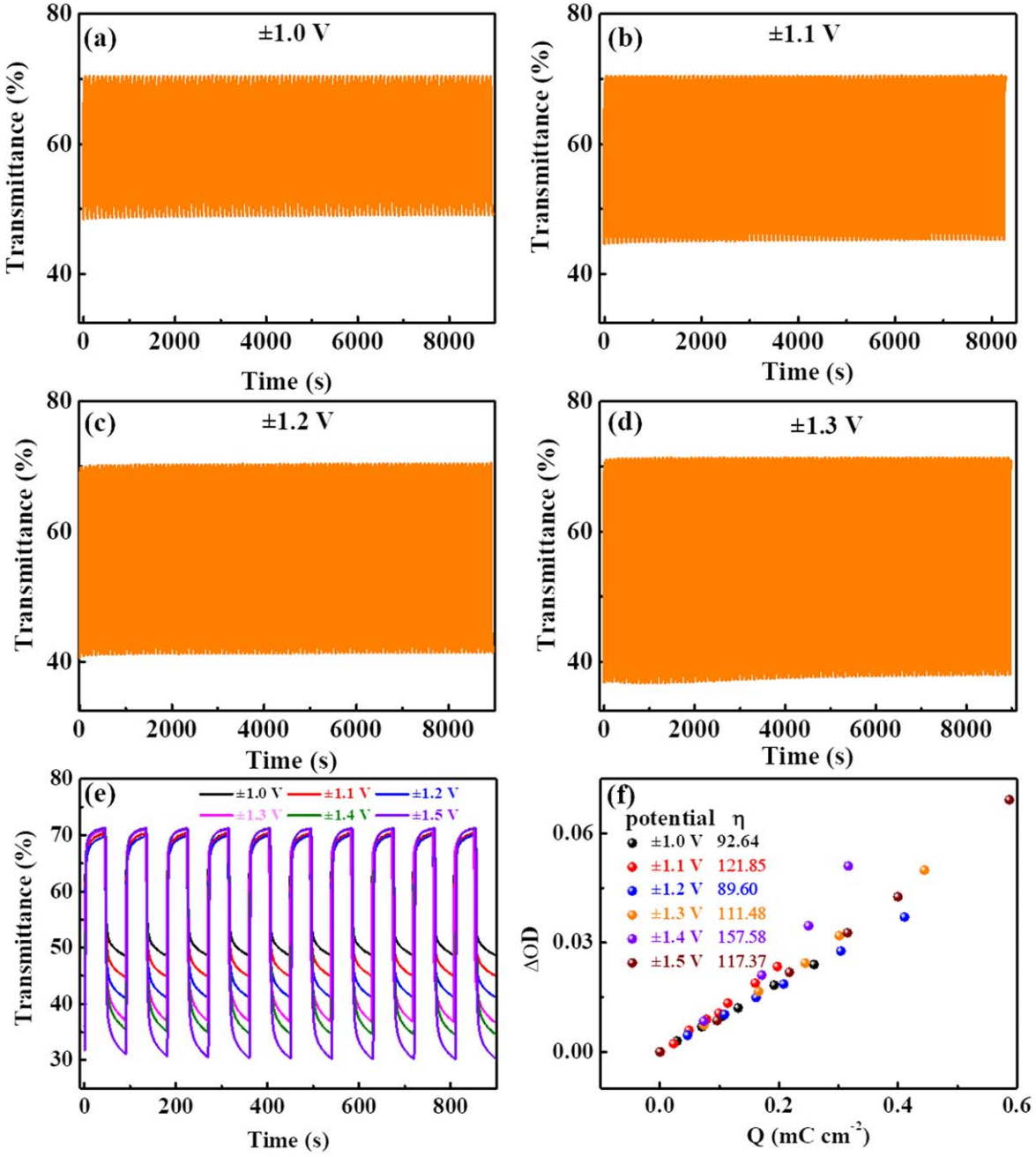

Figure 4. In situ time-dependent optical transmittance spectra at λ_{633} nm (90 s per cycle) of the WO_3-NiO ECD in the 0.10 M PC-$LiClO_4$ with H_2O (volume ratio 100:1) applied the potential of (a) −1.0 V/1.0 V, (b) −1.1 V/1.1 V, (c) −1.2 V/1.2 V and (d) −1.3 V/1.3 V. (e) In situ time-dependent optical transmittance spectra at λ_{633} nm of the WO_3-NiO ECD under the different potentials. (f) The plots of in situ optical density variation as a function of charge density at λ_{633} nm of the WO_3-NiO ECD under the different potentials.

addition of water into the Li^+-based electrolyte can prove beneficial in mechanistic advancement for high performance and long-term-stable ESCs. Besides, electrical splitting of water begins to occur under the potential window of more than 1.23 V, as the following equation:[50]

$$2H_2O \rightarrow O_2 + 4H^+ + 4e^- \quad [6]$$

Oxygen generated by the reaction of Eq. 6 can result in the degradation of optical stability of the ESCs. The other product (H^+) can inhibit the forward process of Eq. 1, which can also destroy reversibility of the NiO counter electrodes.

Conclusion

In summary, the effect of water on the electrochemical and electrochromic properties of the electron beam evaporated NiO thin films for the complementary WO_3-NiO ESCs was investigated. Our findings confirm the Li^+-based electrolyte with H_2O doping can enhance the reaction kinetics and reversibility, and improve the pseudocapacitance characteristics for the NiO counter electrodes. Interestingly, the complementary WO_3-NiO ESCs under the moderate potential window show a high performance with an excellent rate capability, a high coloration efficiency (157.58 $cm^2\ C^{-1}$) and a superior long-term cyclic stability (over 10,000 cycles). Moreover, the irreversible degradation of the NiO electrodes is observed under the potential of $> +$ 1.23 V due to electrically driven water splitting.

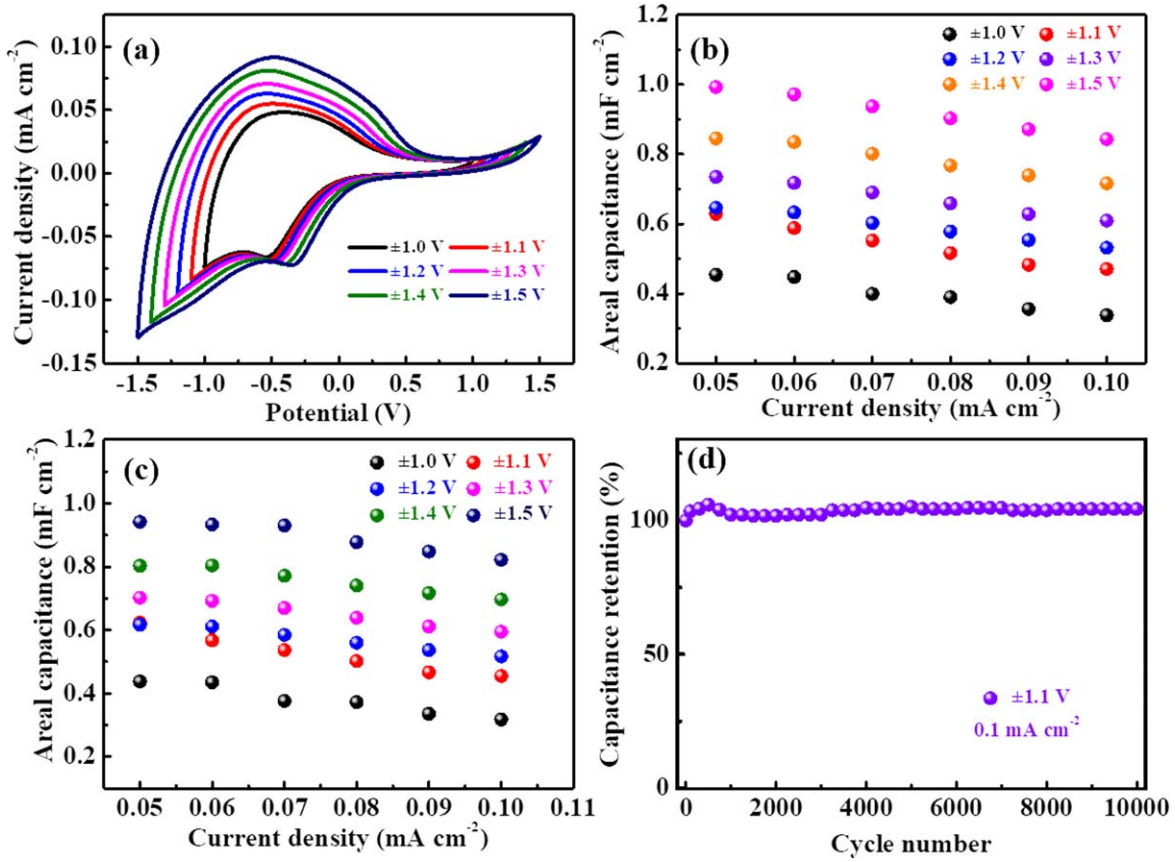

Figure 5. (a) CV curves of the ESCs at 5 mV s^{-1} under various voltage windows. Rate performance of the ESCs at different current density and potential windows in (b) charge and (c) discharge process. (d) The cyclic performance at a current density of 0.1 mA cm^{-2} for the ESCs under ±1.1 V.

Our observations provide new perspectives for developing long-term-stable electrochromic devices embodying nickel oxide.

Acknowledgments

This project is supported by the National Natural Science Foundation of China (61974148 and 61774098) and Ningbo Science and Technology Innovation 2025 Major Special Project (2020Z002).

Declaration of Competing Interest

There are no conflicts to declare.

ORCID

Hongliang Zhang https://orcid.org/0000-0002-9295-8683
Hongtao Cao https://orcid.org/0000-0002-4458-4621

References

1. J. M. Wang, L. Zhang, L. Yu, Z. H. Jiao, H. Q. Xie, X. W. Lou, and X. W. Sun, *Nat. Commun.*, **5**, 4921 (2014).
2. S. Cong, Y. Y. Tian, Q. W. Li, Z. G. Zhao, and F. X. Geng, *Adv. Mater.*, **26**, 4260 (2014).
3. Y. Huang, C. Yang, B. H. Deng, C. Wang, Q. W. Li, C. D. Thibault, K. Huang, K. F. Huo, and H. Wu, *Nano Energy*, **66**, 6 (2019).
4. R. Yuksel, S. Coskun, G. Gunbas, A. Cirpan, L. Toppare, and H. E. Unalan, *J. Electrochem. Soc.*, **164**, A721 (2017).
5. K. Keum, J. W. Kim, S. Y. Hong, J. G. Son, S.-S. Lee, and J. S. Ha, *Adv. Mater.*, **32** (2020).
6. S. L. Zhai, H. E. Karahan, C. J. Wang, Z. X. Pei, L. Wei, and Y. Chen, *Adv. Mater.*, **32**, 19 (2020).
7. Y. Zhou, C. H. Wang, W. Lu, and L. M. Dai, *Adv. Mater.*, **32**, 1902779 (2020).
8. M. Salanne, B. Rotenberg, K. Naoi, K. Kaneko, P. L. Taberna, C. P. Grey, B. Dunn, and P. Simon, *Nat. Energy*, **1**, 10 (2016).
9. K. Wang, H. P. Wu, Y. N. Meng, Y. J. Zhang, and Z. X. Wei, *Energy Environ. Sci.*, **5**, 8384 (2012).
10. M. S. Zhu, Y. Huang, Y. Huang, W. J. Meng, Q. C. Gong, G. M. Li, and C. Y. Zhi, *J. Mater. Chem. A*, **3**, 21321 (2015).
11. Y. Zhong, Z. S. Chai, Z. M. Liang, P. Sun, W. G. Xie, C. X. Zhao, and W. J. Mai, *ACS Appl. Mater. Inter.*, **9**, 34085 (2017).
12. Q. F. Guo, J. J. Li, B. Zhang, G. M. Nie, and D. B. Wang, *ACS Appl. Mater. Inter.*, **11**, 6491 (2019).
13. T. Y. Yun, X. Li, S. H. Kim, and H. C. Moon, *ACS Appl. Mater. Inter.*, **10**, 43993 (2018).
14. J. Chen, Z. Wang, Z. G. Chen, S. Cong, and Z. G. Zhao, *Nano Lett.*, **20**, 1915 (2020).
15. Y. Huang, M. S. Zhu, Y. Huang, Z. X. Pei, H. F. Li, Z. F. Wang, Q. Xue, and C. Y. Zhi, *Adv. Mater.*, **28**, 8344 (2016).
16. M. J. Zhi, C. C. Xiang, J. T. Li, M. Li, and N. Q. Wu, *Nanoscale*, **5**, 72 (2013).
17. Y. L. Chen, Y. Wang, P. Sun, P. H. Yang, L. H. Du, and W. J. Mai, *J. Mater. Chem. A*, **3**, 20614 (2015).
18. W. Zhang, H. Z. Li, E. Hopmann, and A. Y. Elezzabi, *Nanophotonics*, **10**, 825 (2021).
19. J. Kim, A. I. Inamdar, Y. Jo, S. Cho, A. A. Ahmed, B. Hou, S. Cha, T. G. Kim, H. Kim, and H. Im, *J. Mater. Chem. A*, **8**, 13459 (2020).
20. K. Wang, Q. Meng, Q. Wang, W. Zhang, J. Guo, S. Cao, A. Y. Elezzabi, W. W. Yu, L. Liu, and H. Li, *Adv. Energy Sustain. Res.*, **2021**, 2100117 (2021) .
21. H. Z. Li, W. Zhang, and A. Y. Elezzabi, *Adv. Mater.*, **32**, 2003574 (2020).
22. H. Z. Li and A. Y. Elezzabi, *Nanoscale Horiz.*, **5**, 691 (2020).
23. L. Wang, M. Guo, J. Zhan, X. Jiao, D. Chen, and T. Wang, *J. Mater. Chem. A*, **8**, 17098 (2020).
24. K. L. Zhou, H. Wang, J. T. Jiu, J. B. Liu, H. Yan, and K. Suganuma, *Chem. Eng. J.*, **345**, 290 (2018).
25. M. S. Kolathodi, M. Palei, and T. S. Natarajan, *J. Mater. Chem. A*, **3**, 7513 (2015).
26. M. J. Wang, X. F. Song, S. G. Dai, W. N. Xu, Q. Yang, J. L. Liu, C. G. Hu, and D. P. Wei, *Electrochim. Acta*, **214**, 68 (2016).
27. S. T. Li, Y. A. Duan, Y. Teng, N. Fan, and Y. Q. Huo, *Appl. Surf. Sci.*, **478**, 247 (2019).
28. G. F. Cai, X. Wang, M. Q. Cui, P. Darmawan, J. X. Wang, A. L. S. Eh, and P. S. Lee, *Nano Energy*, **12**, 258 (2015).
29. S. Y. Kim, T. Y. Yun, K. S. Yu, and H. C. Moon, *ACS Appl. Mater. Inter.*, **12**, 51978 (2020).
30. Y. Yokoiwa, Y. Abe, M. Kawamura, K. H. Kim, and T. Kiba, *Jpn. J. Appl. Phys.*, **58** (2019).
31. Y. Abe, H. Ueta, T. Obata, M. Kawamura, K. Sasaki, and H. Itoh, *Jpn. J. Appl. Phys.*, **49**, 115802 (2010).

32. C. Xiao, P. Shi, W. Yan, L. Chen, L. Qian, and S. H. Kim, *Colloid. Inter.*, **3**, 55 55 (2019) .
33. C. Xu, C. Ma, X. Kong, and M. Taya, *Polym. Adv. Technol.*, **20**, 178 (2009).
34. W. D. He, C. G. Wang, H. Q. Li, X. L. Deng, X. J. Xu, and T. Y. Zhai, *Adv. Energy Mater.*, **7**, 1700983 (2017).
35. X. H. Xia, J. P. Tu, J. Zhang, X. L. Wang, W. K. Zhang, and H. Huang, *Sol. Energy Mater. Sol. Cells*, **92**, 628 (2008).
36. S. Zhang, S. Cao, T. Zhang, and J. Y. Lee, *Adv. Mater.*, **32**, 2004686 (2020).
37. F. F. Wang, N. Zhang, X. D. Zhao, L. X. Wang, J. Zhang, T. S. Wang, F. F. Liu, Y. C. Liu, and L. Z. Fan, *Adv. Sci.*, **6**, 10 (2019).
38. R. Li et al., *ACS Nano*, **12**, 3759 (2018).
39. K. L. Zhou, H. Wang, Y. Z. Zhang, J. B. Liu, and H. Yan, *J. Electrochem. Soc.*, **163**, H1033 (2016).
40. J. Wang, J. Polleux, J. Lim, and B. Dunn, *J. Phys. Chem. C*, **111**, 14925 (2007).
41. X. Zhang, J. Zhang, S. Kong, K. Zhu, J. Yan, K. Ye, G. Wang, K. Cheng, L. Zhou, and D. Cao, *J. Mater. Chem. A*, **7**, 2855 (2019).
42. Z. Luo, L. Liu, X. Yang, X. Luo, P. Bi, Z. Fu, A. Pang, W. Li, and Y. Yi, *ACS Appl. Mater. Inter.*, **12**, 39098 (2020).
43. K. R. Li, Y. L. Shao, S. Y. Liu, Q. H. Zhang, H. Z. Wang, Y. G. Li, and R. B. Kaner, *Small*, **13**, 1700380 (2017).
44. Z. G. Hou, M. F. Dong, Y. L. Xiong, X. Q. Zhang, Y. C. Zhu, and Y. T. Qian, *Adv. Energy Mater.*, **10**, 1903665 (2020).
45. K. Wang, D. Qiu, H. L. Zhang, G. X. Chen, W. P. Xie, K. Tao, S. H. Bao, L. Y. Liang, J. H. Gao, and H. T. Cao, *J. Sci.-Adv. Mater. Dev.*, **6**, 494 (2021).
46. M. S. Javed, S. G. Dai, M. J. Wang, D. L. Guo, L. Chen, X. Wang, C. U. Hu, and Y. Xi, *J. Power Sources*, **285**, 63 (2015).
47. K. Wang, S. Gao, Z. L. Du, A. B. Yuan, W. Lu, and L. W. Chen, *J. Power Sources*, **305**, 30 (2016).
48. H. Chen, M. Zhou, Z. Wang, S. Y. Zhao, and S. Y. Guan, *Electrochim. Acta*, **148**, 187 (2014).
49. K. Wang, H. L. Zhang, G. X. Chen, T. Tian, K. Tao, L. Y. Liang, J. H. Gao, and H. T. Cao, *J. Alloy. Compd.*, **861**, 158534 (2021).
50. P. T. Babar, A. C. Lokhande, M. G. Gang, B. S. Pawar, S. M. Pawar, and J. H. Kim, *J. Ind. Eng. Chem.*, **60**, 493 (2018).